Discontinuities in Finlines on Semiconductor Substrate

KERSTIN UHDE

Abstract—**Using the singular integral equation (SIE) technique, two finline structures on an insulator–semiconductor substrate are analyzed. The complex propagation constants of the dominant and the first three higher order modes are presented depending on the conductivity of the semiconductor layer. Then, discontinuities in both slot width and substrate complex dielectric constant are investigated theoretically. The reflection and the transmission coefficients of the dominant mode are calculated showing that a step in the permittivity can almost be compensated for by a step in the slot width.**

I. Introduction

WITH THE INCREASING use of the millimeter-wave band and the rapid development of monolithic integrated circuits, there has been a growing interest in the properties of microwave devices on semiconductor substrates. A semiconductor dielectric waveguide has been investigated which is used to realize an optically controlled phase shifter [1]–[3]. The performance of optoelectronic microstrip switches has been studied [4]–[6] and microstrip lines on semiconductor substrates have been analyzed [7]–[9].

Another important structure in the millimeter-wave band is the unilateral finline. Using a finline on an insulator–semiconductor substrate with the fins located at the air–insulator interface, slow-wave modes can be obtained [10], which may be utilized to build delay lines or phase shifters. Taking a slot pattern on a semiconductor substrate, an optoelectronic switch or phase shifter can be realized if the slot region is illuminated by a laser beam. Due to the high field concentration in the slot, this structure seems to be superior to others using alternative transmission media [1]–[3].

Referring to the conductivity of the semiconductor material, an attenuation of the dominant mode has to be expected. Therefore, we propose a structure with a thin semiconductor layer on a lossless dielectric substrate to realize an optoelectronic finline switch. Illumination of the semiconductor layer increases its conductivity and the desired attenuation of the dominant mode can be obtained. In the other case without illumination, small insertion loss can be achieved. Still, the active section should be as short as possible. To prove the distortion caused by this step in the substrate dielectric constants, such a discontinuity has to be analyzed. In this paper, discontinuities in both slot width and substrate dielectric constant are investigated.

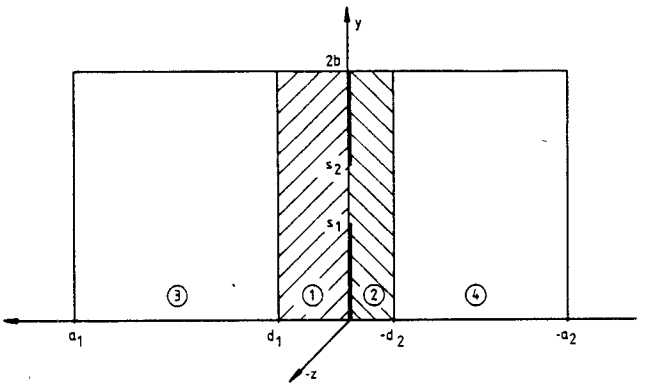

Fig. 1. Finline on a double-layer substrate with the fins located between the two layers. $a_1 + a_2 = 7.112$ mm, and $a_1 = 2b = 3.556$ mm.

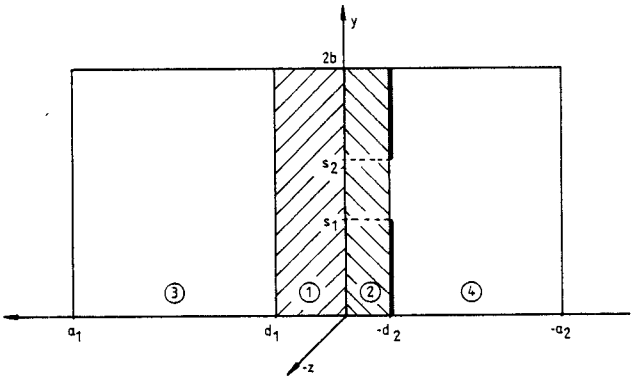

Fig. 2 Finline on a double-layer substrate with the fins located at one side of the substrate. $a_1 + a_2 = 7.112$ mm, $a_1 + d_2 = 2b = 3.556$ mm.

Dispersion in finlines is usually studied using the spectral-domain technique [11]–[13]. Recently, it has been shown that the singular integral equation (SIE) technique is numerically more efficient if, in addition, higher order modes have to be determined [14], [15]. Matching the transverse electromagnetic fields in the plane of a discontinuity may require as many as ten eigenmodes; hence, we have chosen the SIE technique for their calculation.

Step discontinuities in the slot width of a finline have already been analyzed (see, e.g., [16]–[18]). Using a scattering matrix representation, we have adopted the procedure outlined in [17] and generalized it to include the double

Manuscript received March 12, 1986; revised May 30, 1986.

The author is with Technische Universität Hamburg-Harburg, Arbeitsbereich Hochfrequenztechnik, D-2100 Hamburg 90, West-Germany.

IEEE Log Number 8610827.

0018-9480/86/1200-1499$01.00 ©1986 IEEE

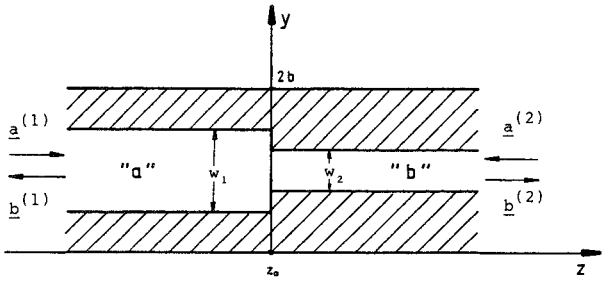

Fig. 3. Step discontinuity in the slot width.

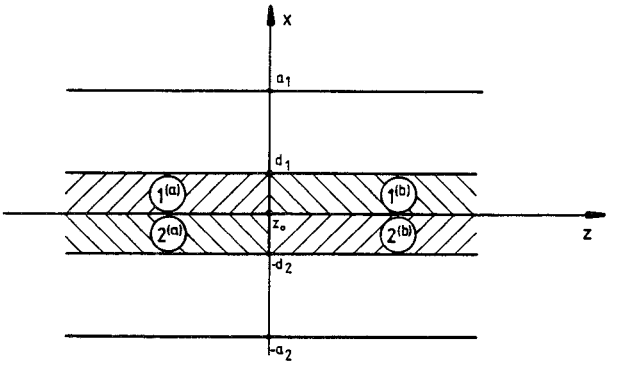

Fig. 4. Abrupt change in the dielectric constants.

discontinuity for a finline on a layered semiconductor substrate.

Two different cross sections have been investigated: a sandwich structure (Fig. 1), where the metal fins are located between two layers, and a structure with the fins located at one side of a double-layer substrate (Fig. 2). The complex propagation constants γ of both structures have been calculated and the influence of some design parameters such as thickness and conductivity of the semiconductor layer on γ has been studied.

The discontinuities to be dealt with are shown in Fig. 3 for an abrupt change in the slot width and in Fig. 4, where the complex dielectric constants are assumed to change abruptly in a certain transverse plane, e.g., the latter may be the intersection between a finline on a double-layer and a finline on a single-layer substrate. Treating both together demonstrates that a destructive interference of both partial reflections is possible and a broad-band input matching can thus be obtained.

II. Analysis of Finlines on an Insulator–Semiconductor Substrate

The finline structures to be analyzed consist of four different regions. Regions 1 and 2 are characterized by their complex permittivities ϵ_{ri}^* with

$$\epsilon_{ri}^* = \epsilon_{ri} - j\frac{\sigma_i}{\omega\epsilon_0}, \qquad \text{for } i=1,2$$

where ϵ_{ri} signifies the dielectric constant and σ_i the conductivity of the region ($i=1,2$). Regions 3 and 4 are air-filled with

$$\epsilon_{ri}^* = 1, \qquad \text{for } i=3,4.$$

The metal fins are assumed to be infinitesimally thin and perfectly conducting. Moreover, it is assumed that all field components have the time and z-dependence $\exp(j\omega t - \gamma z)$, where γ means the complex propagation constant

$$\gamma = \alpha + j\beta.$$

The hybrid field is constructed by superposing an LSE (superscript "h") with an LSM (superscript "e") term [14], which are each described by four scalar potentials ($\psi_i^{e,h}$) satisfying the Helmholtz equation in their respective regions

$$\frac{\partial^2\psi_i^{e,h}}{\partial x^2} + \frac{\partial^2\psi_i^{e,h}}{\partial y^2} + \left(\epsilon_{ri}k_0^2 + \gamma^2\right)\psi_i^{e,h} = 0.$$

Taking the perfect conducting walls at $x=-a_1$, a_2 and $y=0$, $2b$ into account, formulations for the scalar potentials are set up. Applying the interface conditions leads to expressions for the Fourier series expansion coefficients F_n^e and F_n^h of the LSM and LSE Green's functions, respectively.

The tangential electric-field components E_z^e, E_y^h in the slot region and the surface current density components J_z^e, J_y^h on the fins are written as

$$E_z^e = \sum_{n=1}^{\infty} A_n^e \sin\left(\frac{n\pi y}{b}\right)$$

$$E_y^h = \sum_{n=0}^{\infty} A_n^h \cos\left(\frac{n\pi y}{b}\right)$$

$$J_z^e = j\omega\epsilon_0 \sum_{n=1}^{\infty} F_n^e A_n^e \sin\left(\frac{n\pi y}{b}\right)$$

$$J_y^h = \frac{1}{j\omega\mu_0} \sum_{n=0}^{\infty} F_n^h A_n^h \cos\left(\frac{n\pi y}{b}\right).$$

By superposing the LSM with the LSE part, the tangential electric field $\boldsymbol{E}_{ta}$ in the slot region and the surface current density $\boldsymbol{J}_s$ on the fins are determined

$$\boldsymbol{E}_{ta} = \boldsymbol{e}_y\left[\frac{-1}{\gamma}\frac{dE_z^e}{dy} + E_y^h\right] + \boldsymbol{e}_z\left[E_z^e + \frac{1}{\gamma}\frac{dE_y^h}{dy}\right]$$

$$\boldsymbol{J}_s = \boldsymbol{e}_y\left[\frac{-1}{\gamma}\frac{dJ_z^e}{dy} + J_y^h\right] + \boldsymbol{e}_z\left[J_z^e + \frac{1}{\gamma}\frac{dJ_y^h}{dy}\right].$$

$\boldsymbol{e}_y$ and $\boldsymbol{e}_z$ mean the unit vectors in the y- and z-direction, respectively.

Next, two cosine-series $f_1(y)$ and $f_2(y)$ are constructed in terms of $\boldsymbol{E}_{ta}$

$$f_1(y) = \sum_{n=0}^{\infty} A_n^{(1)} \cos\left(\frac{n\pi y}{b}\right) = \frac{dE_z}{dy}$$

$$f_2(y) = \sum_{n=0}^{\infty} A_n^{(2)} \cos\left(\frac{n\pi y}{b}\right) = \frac{1}{j\omega\mu_0}\left[\left(k_0^2 + \gamma^2\right)E_y + \gamma\frac{dE_z}{dy}\right].$$

Then, two sine-series $g_1(y)$ and $g_2(y)$ are defined. $g_1(y)$ consists of two parts with one part $f_3(y)$ depending

on the surface current density J_s and the other containing the expansion coefficients $A_n^{(1)}$. $g_2(y)$ is equally defined using $f_4(y)$ and the expansion coefficients $A_n^{(2)}$

$$g_1(y) = \sum_{n=1}^{\infty} A_n^{(1)} \sin\left(\frac{n\pi y}{b}\right) - f_3(y)$$

$$g_2(y) = \sum_{n=1}^{\infty} A_n^{(2)} \sin\left(\frac{n\pi y}{b}\right) - f_4(y).$$

The sine-series $f_3(y)$ and $f_4(y)$ are constructed in a way that their expansion coefficients $A_n^{(3)}$ and $A_n^{(4)}$ approach $A_n^{(1)}$ and $A_n^{(2)}$, respectively,

$$\lim_{n\to\infty} \left(A_n^{(1)} - A_n^{(3)}\right) = 0$$

$$\lim_{n\to\infty} \left(A_n^{(2)} - A_n^{(4)}\right) = 0$$

with

$$f_3(y) = \sum_{n=1}^{\infty} A_n^{(3)} \sin\left(\frac{n\pi y}{b}\right)$$

$$= \left[-\left(K^h\gamma^2 + K^e k_0^2\right) J_z + \gamma K^h \frac{dJ_y}{dy}\right] \Big/ \left(j\omega\epsilon_0 K^e K^h\right)$$

$$f_4(y) = \sum_{n=1}^{\infty} A_n^{(4)} \sin\left(\frac{n\pi y}{b}\right)$$

$$= \left[\gamma\left(K^e - K^h\right) J_z + K^h\left(\frac{dJ_y}{dy}\right)\right] \Big/ \left(K^e K^h\right).$$

K^e and K^h are given by

$$\lim_{n\to\infty} F_n^e = \frac{K^e}{(n\pi/b)}$$

$$\lim_{n\to\infty} F_n^h = K^h(n\pi/b).$$

Thus, $g_1(y)$ and $g_2(y)$ have asymptotically vanishing coefficients and they may be truncated after the Nth term.

The tangential electric field E_{ta} exists only in the slot region while the surface current density J_s is unequal to zero on the fins. The Fourier series expansion coefficients $A_n^{(1)}$ and $A_n^{(2)}$ are determined in terms of integrals of $f_1(y)$ and $f_2(y)$, respectively. Using these relations leads to two integral equations between $f_1(y)$, $f_2(y)$ and $g_1(y)$, $g_2(y)$. The integral equations are of standard singular type and their solutions are well known (see, e.g., [19]). Thus, $f_1(y)$ and $f_2(y)$ are described by finite sums with $n \leqslant N$ terms. Substituting them in the integrals which determine their coefficients results in a finite, homogeneous system of linear equations with analytically known coefficients from which the complex propagation constant and the field expansion coefficients can be calculated [15].

III. Scattering Matrix Representation of Discontinuities in Finlines

To analyze a discontinuity in the slot width w and in the complex permittivity, the transverse electric- and magnetic-field components $E_{tr}^{(a,b)}$ and $H_{tr}^{(a,b)}$ of the waveguides (a, b) are written in terms of the amplitude vectors of the incident $(a^{(1)}, a^{(2)})$ and scattered $(b^{(1)}, b^{(2)})$ modes

$$E_{tr}^{(a)} = \sum_{i=1}^{N} \left[a_i^{(1)} e^{-\gamma_{ai}(z-z_0)} + b_i^{(1)} e^{\gamma_{ai}(z-z_0)}\right] e_i^{(a)}$$

$$H_{tr}^{(a)} = \sum_{i=1}^{N} \left[a_i(1) e^{-\gamma_{ai}(z-z_0)} - b_i(1) e^{\gamma_{ai}(z-z_0)}\right] h_i^{(a)}$$

$$E_{tr}^{(b)} = \sum_{j=1}^{M} \left[b_j^{(2)} e^{-\gamma_{bj}(z-z_0)} + a_j^{(2)} e^{\gamma_{bj}(z-z_0)}\right] e_j^{(b)}$$

$$H_{tr}^{(b)} = \sum_{j=1}^{M} \left[b_j^{(2)} e^{-\gamma_{bj}(z-z_0)} - a_j^{(2)} e^{\gamma_{bj}(z-z_0)}\right] h_j^{(b)}.$$

γ_{ai} and γ_{bj} represent the propagation constants, and $e_{i,j}^{(a,b)}$ and $h_{i,j}^{(a,b)}$ the electric- and magnetic-field vectors of the ith and jth normal modes, respectively. Then, E_{tr} and H_{tr} are matched in the plane of the discontinuity

$$\int_{(S_a)} \left(E_{tr}^{(a)} \times h_m^{(a)}\right) ds = \int_{(S_b)} \left(E_{tr}^{(b)} \times h_m^{(a)}\right) ds$$

$$\int_{(S_b)} \left(e_n^{(b)} \times H_{tr}^{(a)}\right) ds = \int_{(S_b)} \left(e_n^{(b)} \times H_{tr}^{(b)}\right) ds.$$

Using the following orthogonality relations between the normal modes of an uniform lossyly filled waveguide [20]:

$$\int_{(S_a)} \left(e_n^{(a)} \times h_m^{(a)}\right) ds = P_n \delta_{nm}$$

$$\int_{(S_b)} \left(e_n^{(b)} \times h_m^{(b)}\right) ds = Q_m \delta_{mn}$$

and with the definition

$$A_{mn} = \int_{(S_b)} \left(e_n^{(b)} \times h_m^{(a)}\right) ds$$

relations between the above-mentioned amplitude vectors are obtained. S_a and S_b are the cross sections of the waveguides (a, b) and δ_{nm} is the Kronecker delta. To calculate P_n, Q_m, and A_{mn}, four terms referring to the different regions $(i = 1, \cdots, 4)$ have to be taken into account, e.g.,

$$A_{mn} = \int_0^{2b} \left[\int_{-d_1}^{0} \left(e_{n1}^{(b)} \times h_{m1}^{(a)}\right) dx + \int_0^{d_2} \left(e_{n2}^{(b)} \times h_{m2}^{(a)}\right) dx + \int_{-a_1}^{-d_1} \left(e_{n3}^{(b)} \times h_{m3}^{(a)}\right) dx + \int_{d_2}^{a_2} \left(e_{n4}^{(b)} \times h_{m4}^{(a)}\right) dx\right] dy.$$

This leads to a system of $N + M$ linear equations in the amplitude vectors

$$P_i\left(a_i^{(1)} + b_i^{(1)}\right) = \sum_{j=1}^{M} A_{ij}\left(b_j^{(2)} + a_j^{(2)}\right), \qquad i = 1, \cdots, N$$

$$\sum_{i=1}^{N} A_{ij}\left(a_i^{(1)} - b_i^{(1)}\right) = Q_j\left(b_j^{(2)} - a_j^{(2)}\right), \qquad j = 1, \cdots, M.$$

These equations can be arranged so that the discontinuity is described in a scattering matrix representation [17]

$$\begin{bmatrix} b^{(1)} \\ b^{(2)} \end{bmatrix} = \begin{bmatrix} S_{11} & S_{12} \\ S_{21} & S_{22} \end{bmatrix} \begin{bmatrix} a^{(1)} \\ a^{(2)} \end{bmatrix}.$$

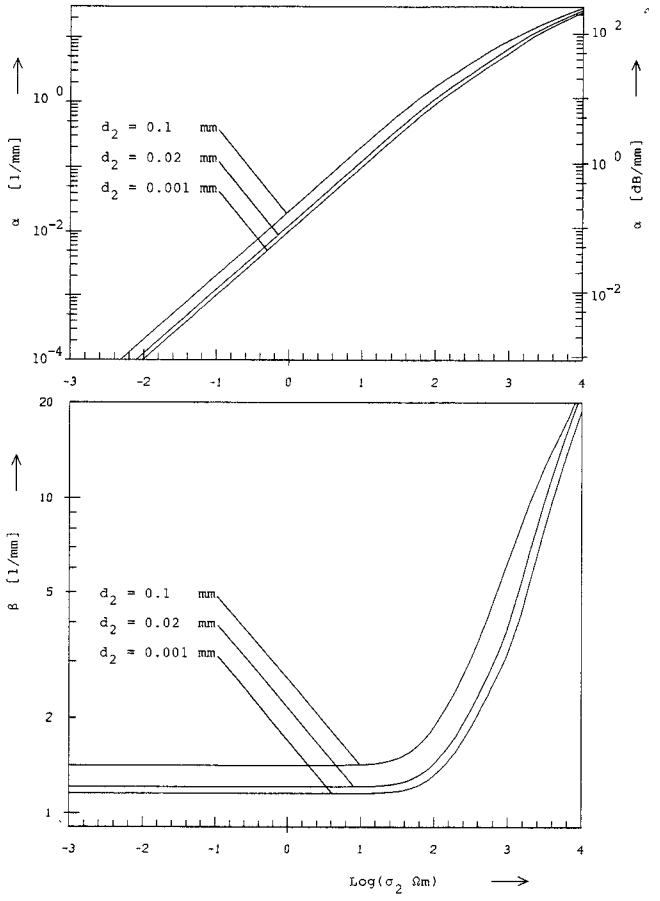

Fig. 5. α and β of the dominant mode versus conductivity σ_2, using the structure shown in Fig. 1. Identical quantities for Figs. 5, 6, 8, and 9. $f = 33$ GHz, $w = 0.2$ mm, $d_1 = 0.3$ mm, $\epsilon_{r1} = 4.0$, $\epsilon_{r2} = 12.0$, and $\sigma_1 = 0$.

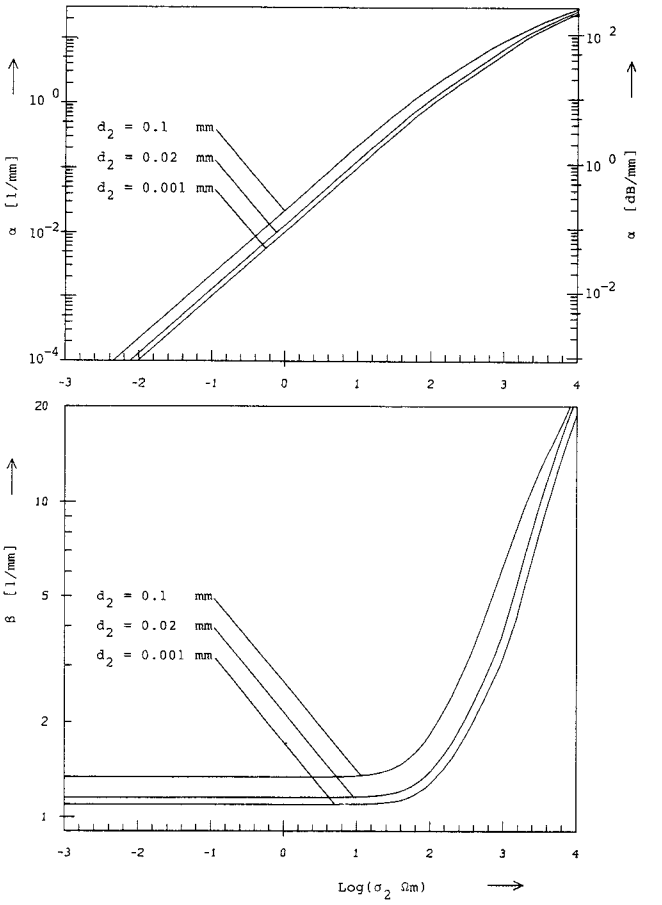

Fig. 6. α and β of the dominant mode versus σ_2 (structure of Fig. 2).

The submatrices $[S_{11}]$, $[S_{12}]$, $[S_{21}]$, and $[S_{22}]$ have been calculated according to [17]. In the following section, results will be given for both the reflection and the transmission coefficients of the dominant mode.

IV. Numerical Results

A. Calculation of the Propagation Constant

First, the propagation constants of a finline on an insulator semiconductor substrate have to be determined. It is assumed that the substrate consists of a lossless silicon oxide layer ($\epsilon_{r1} = 4.0, \sigma_1 = 0$) and a conducting silicon layer ($\epsilon_{r2} = 12.0, \sigma_2$). Thereby, two configurations are possible: one with the fins between the two layers (Fig. 1) and the other with the fins located at one side of the double-layer substrate (Fig. 2). The dimensions of the shielding walls have been chosen according to a WR-28 waveguide which is used for 26.5–40 GHz operation. A finline on a thin substrate is difficult to handle. Therefore, we have assumed a thickness of the silicon–oxide layer of 0.3 mm. At a fixed frequency ($f = 33$ GHz), the propagation constants of both structures have been calculated for different thicknesses of the silicon layer depending on the conductivity σ_2. A very similar behavior is observed. Figs. 5 and 6 show the real part α and the imaginary part β of the complex propagation constant γ of the dominant mode. The attenuation coefficient α increases with conductivity. This can be explained by the high field concentration in the slot. A conductivity of the layer next to the fins must have a considerable influence. In comparison to the reactive attenuation that occurs below cutoff, this attenuation is dissipative. The phase coefficient β changes slightly for small values of conductivity. Since the structure shown in Fig. 1 has a dielectric layer on both sides of the fins, a larger value of β is obtained. In the range of high conductivities, β increases strongly, i.e., the wave is slowed down. Then, the field is concentrated in the conducting silicon layer and the attenuation and phase coefficients of both structures have almost the same values. Increasing the thickness of the silicon layer, α and β are enlarged. The increase of β is due to the high value of the relative dielectric constant ϵ_{r2} of silicon, which may lower the cutoff frequency of the next higher order modes. This reduces the usable bandwidth.

Interchanging the sequence of the layers in the structure shown in Fig. 2 leads to a finline with the fins located at the silicon oxide–air interface. This structure has quite different properties. In Fig. 7, α and β of the dominant mode are given versus conductivity σ_1 of silicon for different thicknesses of the silicon layer; α and β increase versus σ_1, reach a maximum value, and decrease again, which means that the slow-wave effect exists in a narrow range of conductivities. Then, the field maximum is shifted to the silicon layer. Thus, the attenuation and phase coefficients are enlarged and the maximum values of both occur at the

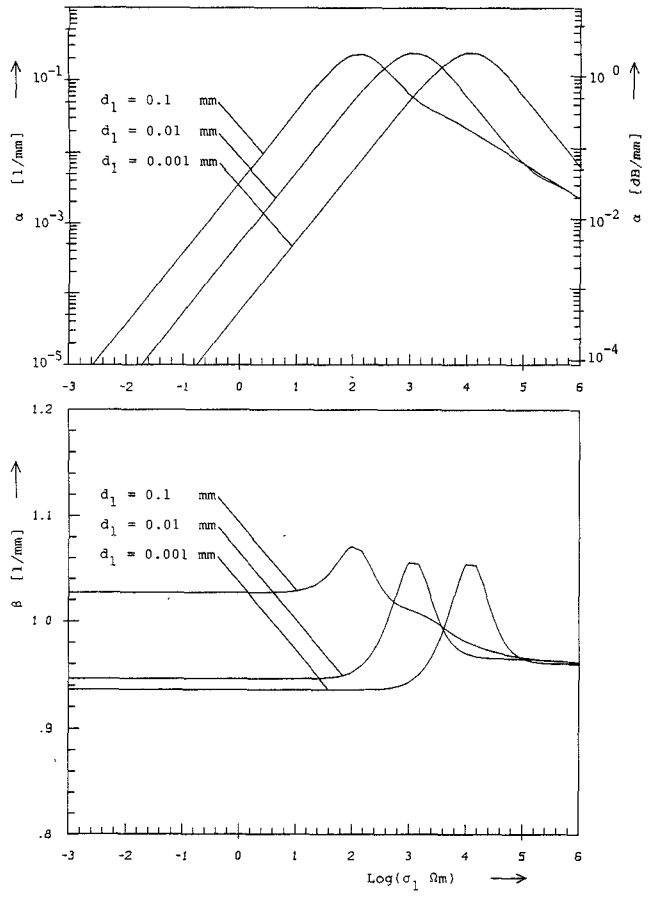

Fig. 7. α and β of the dominant mode versus σ_1 (structure of Fig. 2). $f = 33$ GHz, $w = 0.2$ mm, $d_2 = 0.3$ mm, $\epsilon_{r1} = 12.0$, $\epsilon_{r2} = 4.0$, and $\sigma_2 = 0$.

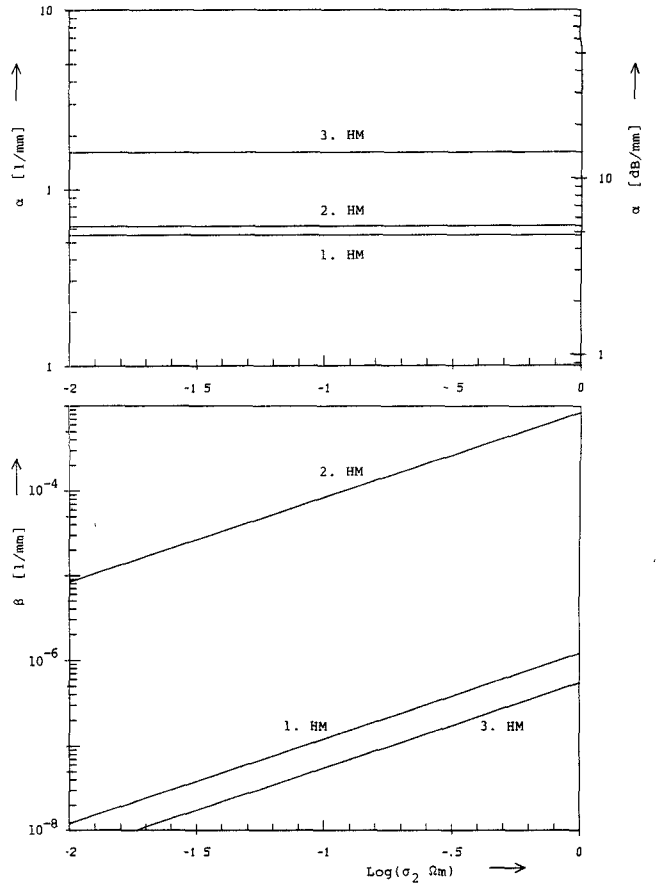

Fig. 8. α and β of the first three higher order modes versus σ_2 (structure of Fig. 1). $d_2 = 0.001$ mm.

same conductivity. Using a thicker silicon layer, the slow-wave effect appears at smaller conductivities. As σ_1 tends to infinity, d_1 has no influence any more, and the three curves of the imaginary part in Fig. 7 have the same asymptotic limit. Such a structure may be used to build phase shifters or delay lines, but it is not suited to realize an optoelectronic finline switch, for the maximum attenuation is about 2 dB/mm.

Only the finline structures in Figs. 5 and 6 will be treated in the following discussion. Taking a conductivity into account, the propagation constants of the higher order modes are also complex. In Figs. 8 and 9, α and β of the first three higher order modes are shown versus the conductivity σ_2 of the silicon layer. In contrast to the propagation constant of the dominant mode, the real part α is slightly affected by the conductivity while the imaginary part β increases versus σ_2. The imaginary part β of the second higher order mode (2. HM) is larger than the imaginary parts of the first and third higher order mode. This is caused by a maximum of the electric field of the 2. HM near the conducting layer.

B. Computed Scattering Parameters

To investigate discontinuities in the slot width and in the substrate dielectric constants, the magnitudes of the reflection and the transmission coefficients ($|S_{11}|$ and $|S_{21}|$) and their phases ($\sphericalangle S_{11}$ and $\sphericalangle S_{21}$) have been calculated. The sandwich structure (see Figs. 1 and 5) is analyzed in

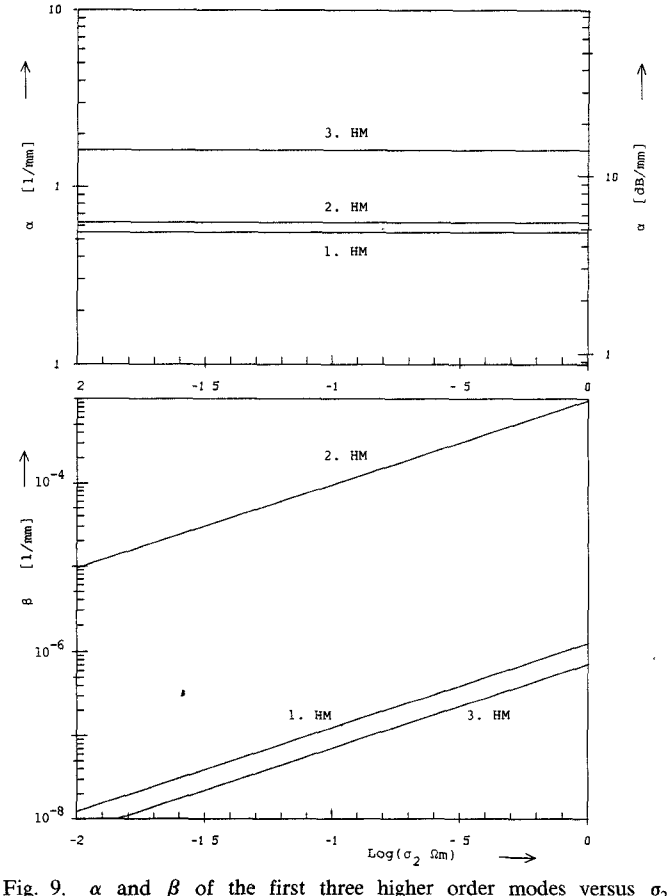

Fig. 9. α and β of the first three higher order modes versus σ_2 (structure of Fig. 2). $d_2 = 0.001$ mm.

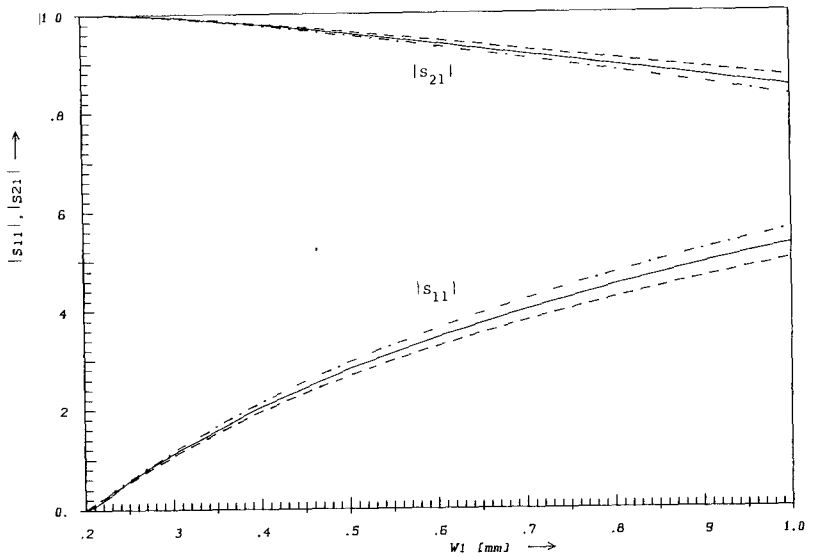

Fig. 10. Slot width dependence of $|S_{11}|$ and $|S_{21}|$ for the structure shown in Fig. 1. $d_2 = 0.1$ mm, $\epsilon_{r2}^{(b)} = 12.0$, $\sigma_2^{(a)} = \sigma_2^{(b)} = 1.0$ $(\Omega m)^{-1}$, $f = 26$ GHz ----, $f = 33$ GHz ——, and $f = 40$ GHz–·–·–·–. Identical quantities for Figs 10–17. $w_2 = 0.2$ mm, $d_1 = 0.3$ mm, $\epsilon_{r1}^{(a)} = \epsilon_{r1}^{(b)} = 4.0$, $\epsilon_{r2}^{(a)} = 12.0$, and $\sigma_1^{(a)} = \sigma_1^{(b)} = 0$.

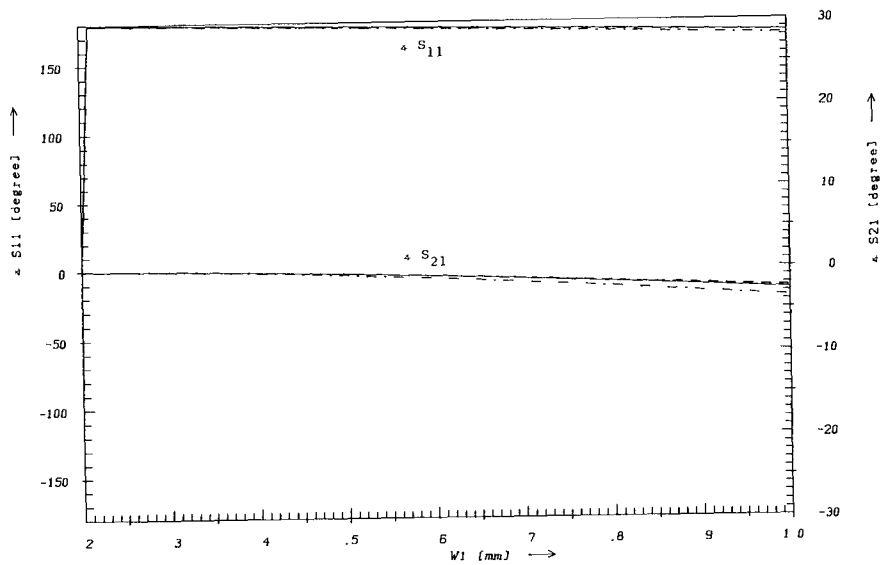

Fig. 11. Phases of S_{11} and S_{21} versus w_1 using the same quantities as in Fig. 10. $f = 26$ GHz ----, $f = 33$ GHz ——, and $f = 40$ GHz – · – · –.

Figs. 10–14. The computed values of S_{11} and S_{21} of the structure shown in Figs. 2 and 6 are given in Figs. 15–17.

First, a step discontinuity in the slot width has been studied. The substrate is assumed to consist of a lossless and a conducting layer. In Fig. 10, $|S_{11}|$ and $|S_{21}|$ are presented versus slot width w_1 of waveguide "a" at three frequency points. $|S_{11}|$ tends to larger values versus w_1 while $|S_{21}|$ is decreased. This is quite similar to the behavior of step discontinuities in finlines on a lossless single-layer substrate. Increasing the step in the slot width causes a stronger reflection. At small values of w_1, almost no frequency dependence can be observed. At larger values of w_1, a small influence of the frequency is obtained: $|S_{11}|$ is enlarged versus the frequency. The phases of S_{11} and S_{21} are given in Fig. 11. The phase of S_{21} is slightly influenced versus w_1 while the phase of S_{11} turns from 0 to 180°. This is due to the negative value of the real part of S_{11}. The frequency dependence of both is small. Calculating the reflection and the transmission coefficients of the structure in Fig. 2 leads to almost the same results.

The intersection between a finline on a double-layer silicon–silicon-oxide substrate and one on a lossless silicon–oxide substrate has been investigated. The abrupt change in the complex permittivities causes a reflection of the dominant mode. Fig. 12 shows S_{11} and S_{21} versus conductivity $\sigma_2^{(a)}$ of waveguide "a" for two different thicknesses of the silicon layer. In the considered range of conductivities, $\sigma_2^{(a)}$ has almost no influence on the reflec-

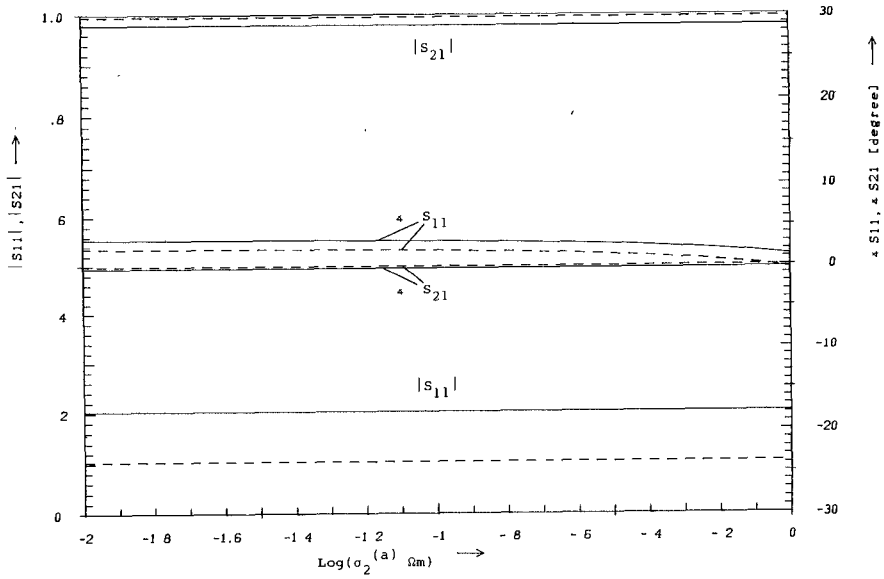

Fig. 12. $|S_{11}|$ and $|S_{21}|$ and phases of S_{11} and S_{21} versus conductivity $\sigma_2^{(a)}$ (structure of Fig. 1). $f = 33$ GHz, $w_1 = 0.2$ mm, $\epsilon_{r2}^{(b)} = 1.0$, $\sigma_2^{(b)} = 0$, $d_2 = 0.001$ mm ----, and $d_2 = 0.1$ mm ———.

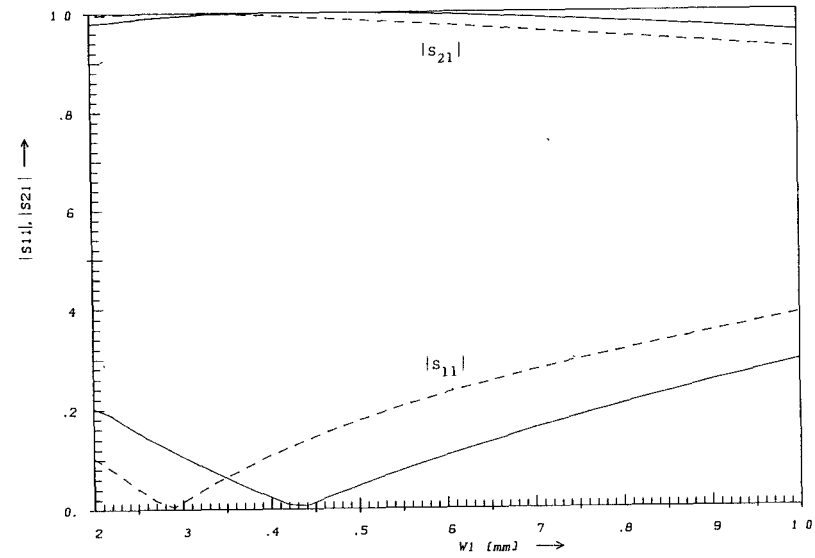

Fig. 13. $|S_{11}|$ and $|S_{21}|$ versus slot width w_1 (structure of Fig. 1). $f = 33$ GHz, $\epsilon_{r2}^{(b)} = 1.0$, $\sigma_2^{(a)} = 1.0$ $(\Omega\text{m})^{-1}$, $\sigma_2^{(b)} = 0$, $d_2 = 0.001$ mm ----, and $d_2 = 0.1$ mm ———.

tion and the transmission coefficients. The reflection is caused mainly by the change in the relative dielectric constants. Increasing the thickness of the silicon layer leads to a stronger reflection, for the distortion of the field is enlarged. The phases of S_{11} and S_{21} are slightly changed by a step in the dielectric constants. Values of about zero degree have been computed, i.e., the real parts of S_{11} and S_{21} are positive. Fig. 15 presents the reflection and transmission coefficients of the structure in Fig. 2 versus $\sigma_2^{(a)}$. Comparing it with Fig. 12, a similar behavior can be seen; however, a smaller value of $|S_{11}|$ is obtained referring to the smaller phase coefficient of this structure (see Figs. 5 and 6).

Finally, both discontinuities are treated together. At fixed conductivity $\sigma_2^{(a)}$, the influence of the slot width w_1 on $|S_{11}|$ and $|S_{21}|$ has been analyzed. As can be seen in Figs. 13 and 16, a minimum of $|S_{11}|$ is obtained. At small values of w_1, the reflection due to the step in the substrate dielectric constants dominates and the real part of S_{11} is positive. Increasing w_1, the real part of S_{11} decreases, passes through zero and tends to large negative values, i.e., both partial reflections interfere destructively at the minimum. In Figs. 14 and 17, the phases of S_{11} and S_{21} are presented versus w_1. The phase of S_{11} turns from 0 to 180°, which is caused by the change of sign of the real part of S_{11}. The phase of S_{21} is slightly affected. Using a thin silicon layer lowers the slot width w_1 at which the minimum appears (see Fig. 13). The frequency dependence of the matching procedure can be studied in Figs. 16 and 17. Only small change in S_{11} and S_{21} is observed. Therefore, a

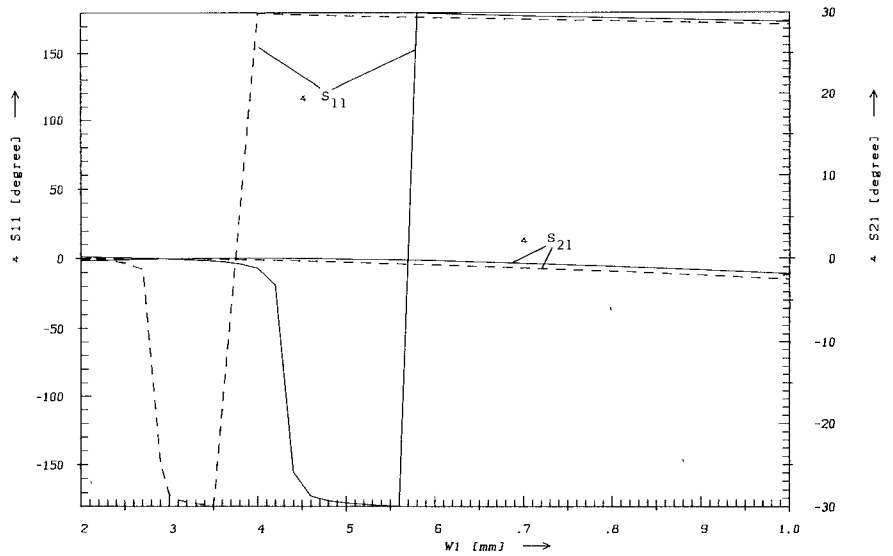

Fig. 14. Phases of S_{11} and S_{21} versus slot width w_1 with the same quantities as in Fig. 13. $d_2 = 0.001$ mm ---- and $d_2 = 0.1$ mm ——.

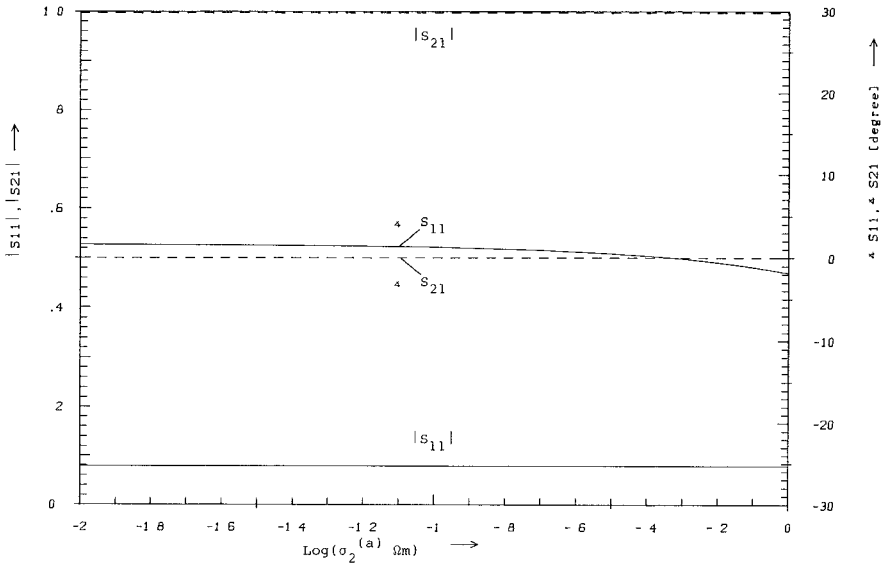

Fig. 15. $|S_{11}|$ and $|S_{21}|$ and phases of S_{11} and S_{21} versus conductivity $\sigma_2^{(a)}$ (structure of Fig. 2). $f = 33$ GHz, $w_1 = 0.2$ mm, $d_2 = 0.001$ mm, $\epsilon_{r2}^{(b)} = 4.0$, and $\sigma_2^{(b)} = 0$.

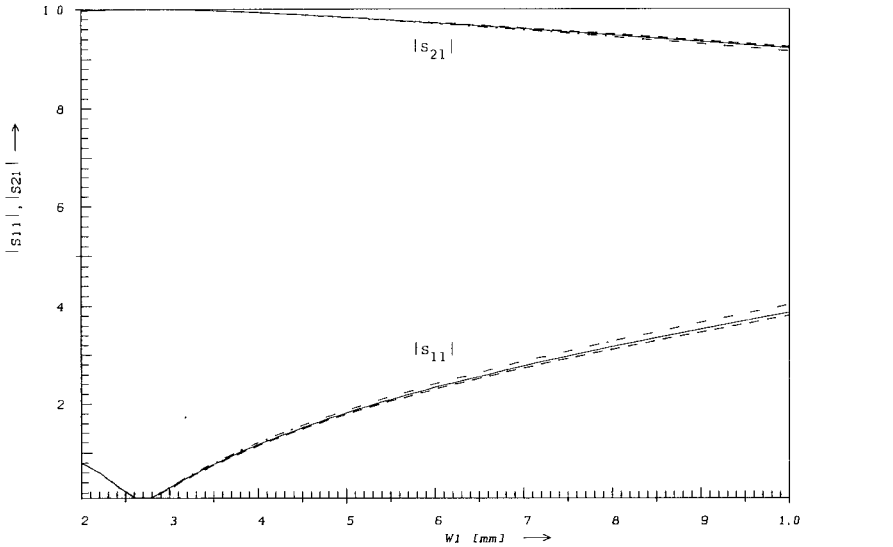

Fig 16. $|S_{11}|$ and $|S_{21}|$ versus slot width w_1 (structure of Fig. 2). $d_2 = 0.001$ mm, $\epsilon_{r2}^{(b)} = 4.0$, $\sigma_2^{(a)} = 1\,0\ (\Omega\text{m})^{-1}$, $\sigma_2^{(b)} = 0$, $f = 26$ GHz ----, $f = 33$ GHz ——, and $f = 40$ GHz – · – · – · –.

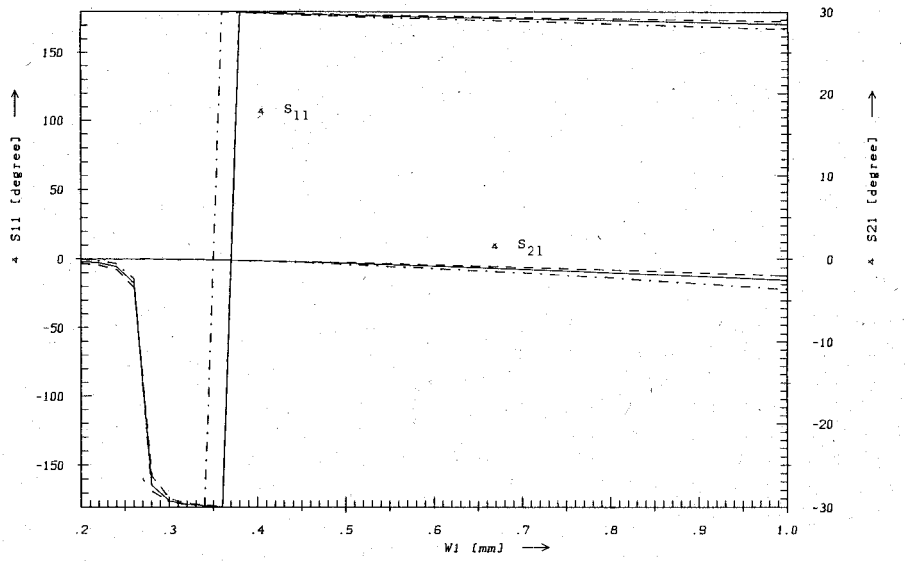

Fig. 17. Phases of S_{11} and S_{21} versus slot width w_1 using the same quantities as in Fig. 16. $f = 26$ GHz ----, $f = 33$ GHz ——, and $f = 40$ GHz – · – · – · –.

reflection occurring at the intersection between two regions with different material constants can be compensated for by a proper step in the slot width. As shown in Figs. 16 and 17 moreover, a broad-band input matching can thus be achieved.

Applying this to the design of an optoelectronic finline switch with a finite semiconductor section, the design parameters as thickness of both layers and intrinsic conductivity of the semiconductor layer have to be chosen. The reflection caused by the step in the dielectric constants and the slot width of the matching point have to be calculated. Thus, the input reflection can be minimized. On the other hand, a strong attenuation of the dominant mode is obtained by increasing the conductivity of the silicon layer e.g., by illuminating it with a laser beam. Therefore, a good performance of such a finline switch can be expected.

References

[1] C. H. Lee, P. S. Mak, and A. P. De Fonzo, "Optical control of millimeter-wave propagation in dielectric waveguides," *IEEE J. Quantum Electron.*, vol. QE-16, pp. 277–288, 1980.

[2] A. M. Vaucher, C. D. Striffler, and C. H. Lee, "Theory of optically controlled millimeter-wave phase shifters," *IEEE Trans. Microwave Theory Tech.*, vol. MTT-31, pp. 209–216, 1983.

[3] A. M. Yurek, M. G. Li, C. D. Striffler, and C. H. Lee, "Modulation of millimeter-waves using diode laser illumination of a silicon waveguide," *Int. J. Infrared Millimeter Waves*, vol. 5, pp. 1381–1388, 1984.

[4] D. H. Auston, "Picosecond optoelectronic switching and gating in silicon," *Appl. Phys. Lett.*, vol. 26, pp. 101–103, 1975.

[5] W. Platte, "Optimum design and performance of optoelectronic sampling components on silicon substrate," *Arch. Elek. Übertragung.*, Band 33, pp. 364–370, 1979.

[6] W. Platte, "Optoelectronic microwave switching via laser-induced plasma tapers in GaAs microstrip sections," *IEEE Trans. Microwave Theory Tech.*, vol. MTT-29, pp. 1010–1018, 1981.

[7] Y. G. Shih and T. Itoh, "Analysis of printed transmission lines for monolithic integrated circuits," *Electron. Lett.*, vol. 9, pp. 585–586, 1982.

[8] Y. Fukuoka, Y. G. Shih, and T. Itoh, "Analysis of slow-wave coplanar waveguides for monolithic integrated circuits," *IEEE Trans. Microwave Theory Tech.*, vol. MTT-31, pp. 567–573, 1983.

[9] T. G. Mu, H. Ogawa, and T. Itoh, "Characteristics of coupled slow-wave microstrip lines," *Electron. Lett.*, vol. 21, pp. 946–947, 1985.

[10] A. Abdel Azeim, H. El Hennawy, and S. Mahrous, "Analysis of fin-lines on semiconductor substrate," in *Proc. 14th EuMC* (Liege, France), 1984, pp. 346–351.

[11] L. P. Schmidt and T. Itoh, "Spectral domain analysis of dominant and higher order modes in fin-lines," *IEEE Trans. Microwave Theory Tech.*, vol. MTT-28, pp. 981–989, 1980.

[12] L. P. Schmidt, T. Itoh, and H. Hofmann, "Characteristics of unilateral fin-line structures with arbitrarily located slots," *IEEE Trans. Microwave Theory Tech.*, vol. MTT-29, pp. 352–355, 1981.

[13] J. B. Knorr and P. M. Shayda, "Millimeter-wave fin-line characteristics," *IEEE Trans. Microwave Theory Tech.*, vol. MTT-28, pp. 737–743, 1980.

[14] A. S. Omar and K. Schünemann, "Space-domain decoupling of LSE and LSM fields in generalized planar guiding structures," *IEEE Trans. Microwave Theory Tech.*, vol. MTT-32, pp. 1626–1632, 1984.

[15] A. S. Omar and K. Schünemann, "Formulation of the singular integral equation technique for planar transmission lines," *IEEE Trans. Microwave Theory Tech.*, vol. MTT-33, pp. 1313–1322, 1985.

[16] R. Sorrentino and T. Itoh, "Transverse resonance analysis of finline discontinuities," *IEEE Trans. Microwave Theory Tech.*, vol. MTT-32, pp. 1633–1638, 1984.

[17] A. S. Omar and K. Schünemann, "Transmission matrix representation of finline discontinuities," *IEEE Trans. Microwave Theory Tech.*, vol. MTT-33, pp. 765–770, 1985.

[18] M. Helard, J. Citerne, O. Picon, and V. F. Hanna, "Theoretical and experimental investigation of finline discontinuities," *IEEE Trans. Microwave Theory Tech.*, vol. MTT-33, pp. 994–1003, 1985.

[19] L. Lewin, *Theory of Waveguides*. London: Newnes Butterworths.

[20] R. E. Collin, *Field Theory of Guided Waves*. New York: McGraw-Hill, 1960.

Kerstin Uhde was born in Wolfenbüttel, Germany, on March 6, 1960. She received the Dipl. Ing. degree in electrical engineering from Technische Universität Braunschweig, Germany, in 1984.

Since then she has been with the Technische Universität Hamburg-Harburg, Germany, where she is working towards the Dr. Ing. degree. Her current research interests are finline structures on semiconductor substrate and optoelectronics.